Penetration Characteristics of a Submerged Steam Jet

P. J. KERNEY, G. M. FAETH, and D. R. OLSON

The Pennsylvania State University, Pennsylvania 16802

An experimental investigation was made of the length of the turbulent vapor cavity formed by a steam jet discharging into a subcooled liquid water bath. The experiments considered both constant area and convergent-divergent steam injectors of various external geometries. The tests were conducted with the bath at atmospheric pressure, bath temperatures in the range 301-358K, injector exit diameters in the range 0.00040-0.0112 m, for choked injector flows having mass velocities in the range 332-2050 $kg/m^2 \cdot s$. These conditions yielded injector exit Reynolds numbers from 2 to 150×10^4. Over this range a correlation was developed to yield the length of the vapor cavity as a function of the injector diameter, exit mass velocity, and a driving potential for the condensation process. The heat transfer coefficients for this condensation process were found to be significantly greater than those encountered in turbulent film condensation processes in the vicinity of tubes and walls.

The phenomena of a condensible gas jet discharging into a liquid bath has attracted attention from investigators representing a number of interests and disciplines. This process may involve condensation of a pure component (steam into water), dissolution of a gas into a bulk liquid phase (ammonia into water), or a more complicated reactive situation (oxidizing gas injected into a liquid metal bath). In each of these systems, it is of interest to know the size and characteristics of the submerged jet cavity as a function of the operating conditions. Since the steam jet condensing into water has experimental advantages due to its relative safety and good optical qualities, the present investigation was limited to this case.

Although numerous studies, for example, (1 to 3) have been conducted on noncondensible gases discharging into water, there have been relatively few studies of the condensing jet. In one of the earliest studies, Boehm (4) observed the cavity formed by a steam jet issuing from a 3-mm. diameter injector into a water bath. He observed that the length of the cavity increased with increasing bath temperature. As the bath approached the saturation temperature, the cavity became unstable and broke up into numerous individual bubbles.

Glikman (5) probed the velocity and temperature distribution in cavities formed from axisymmetric and two dimensional injectors. The data was limited and no attempt was made to correlate the results, however, Glikman concluded that condensation occurs in an irregular wavy interface. Unusually high turbulence levels were estimated in proximity to the interface.

Binford et al. (6) observed cavities formed by steam jets issuing from vertical tubes having inside diameters in the range 0.0109-0.0226m. at atmospheric pressure. Jet exit mass velocities were in the range 58-350 $kg/m^2 \cdot s$ at a fixed bath temperature of 305°K. It was found that the ratio of cavity length to injector diameter varied logarithmically with jet exit mass velocity. A definite change in slope was observed for this correlation when the injector was choked. In the choked flow regime, the growth of cavity length with increasing mass velocity was much more rapid than for unchoked flow.

The goal of the present investigation was to extend the experimental range of these earlier investigations. Particular emphasis was placed on obtaining a correlation for cavity length as a function of operating conditions (bath temperature, injector mass velocity, diameter, etc.). Experimental conditions were limited to choked flows where cavity breakup did not occur. The tests considered injector inside diameters in the range 0.00040-0.0112m, mass velocities in the range 332-2050 $kg/m^2 \cdot s$ with bath temperatures of 301°-352°K. at atmospheric pressure. Constant area and convergent-divergent injectors of various external geometries were considered in the testing.

EXPERIMENTAL APPARATUS AND PROCEDURE

A sketch of the overall test apparatus is shown in Figure 1. The water bath was contained within a rectangular steel tank equipped with windows for observation and photography of the steam cavities. The water bath was 0.76 m high, 0.76 m wide, and 1.52 m. long. The bath temperature was measured by seven thermocouples placed at various locations in the bath. The temperature variation between thermocouples was less than 0.5°K. for most tests, rising to a maximum of 1°K. at the highest steam flow rates tested.

Steam was drawn through a pressure regulator from a local supply maintained at 1.72×10^6 N/m^2. The steam flow rate was measured by critical flow orifices or direct calibration of the injector (for the highest flow rates). A plenum chamber having a volume of 0.025 m.³ was located just upstream of
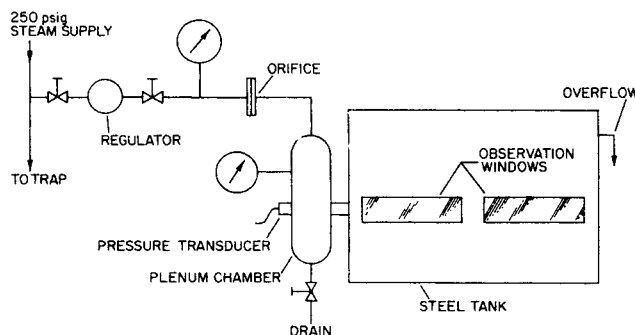
Fig. 1. Schematic diagram of experimental apparatus.

the injector in order to reduce pressure oscillations. Even with the plenum chamber, pressure oscillations (accompanied by separation of the cavity from the injector) were observed when the flow was not choked in the injector. To avoid this, testing was limited to choked flows. The steam supply system and the plenum chamber were electrically heated and insulated to prevent condensation. For all tests, the steam was super-heated 4-6°K. in the plenum chamber. Calculations indicated a moisture content of 3 to 5% at the exit of the injector for these conditions (7).

The geometry of the steam injectors is given in Figure 2. The injectors were mounted in the end wall of the bath. The injector passages were drilled with length to diameter ratios exceeding 16 to insure reasonably well developed flow leaving the injector. Some testing was also done with convergent-divergent injector passages.

The vapor cavity was photographed with a Graphlex camera. The cavity was illuminated with a Strobotac having a flash duration of eight microseconds in order to stop the motion of the cavity for a sharp image. Similar to the findings of others (4 to 6), dissolved gas in the water caused a cloudy flow of fine gas bubbles which obscured cavity photographs. This difficulty was minimized by filling the tank with steam condensate just prior to testing.

The measured cavity lengths are averages of six photographs. Statistical analysis, employing equations for small samples (8), indicates a standard deviation of the results of approximately 10%. A summary of the data for all test conditions is given in Table 1.

THEORETICAL CONSIDERATIONS

Preliminary observations indicated that the shape of the steam cavity was influenced by the exit plane pressure of the injector (7). For exit plane pressures near the ambient pressure (adapted case), the maximum diameter of the cavity was only slightly larger than the injector exit diameter for the conditions tested (this includes both constant area injectors and convergent-divergent injectors). For exit plane pressures greater than the ambient pressure, the cavity diameter rapidly increased near the injector exit, apparently due to the external expansion of the gas leaving the injector. Conversely, for an overexpanded convergent-divergent injector (exit plane pressure below ambient pressure) the cavity diameter tended to contract near the injector exit. Therefore, the effect of the external expansion of the flow leaving the injector on the cavity length must be added to the previously recognized effects of jet diameter, jet exit mass velocity, and bath temperature (4 to 6).

In view of the complexities of the actual phenomena, only a simplified model was attempted for the condensing jet. The purpose of the analysis was to gain understanding of the process and to determine the major physical parameters to aid in data correlation.

The model, consisting of a vapor jet issuing into a stagnant liquid bath, is illustrated in Figure 3. The bulk of the vapor condensation is assumed to be taking place at the gas-liquid interface. The intermittent, irregular interface has been represented by a smooth time-averaged surface.
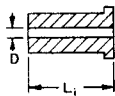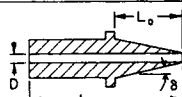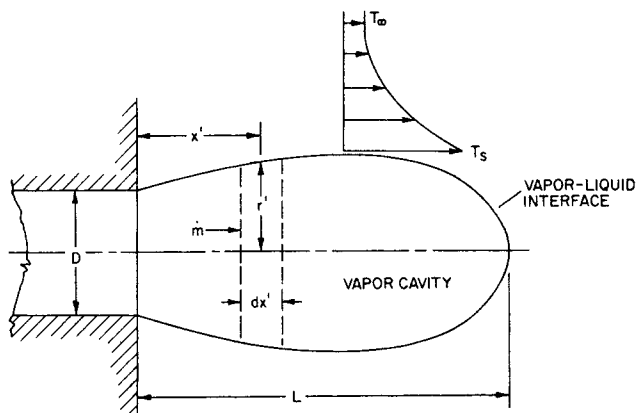

Fig. 3. Schematic of the condensing jet model.

At ordinary pressures, as in the present experiments, phase equilibrium is maintained at the interface. Therefore, neglecting pressure gradients in the liquid phase, the interface temperature equals the saturation temperature of the condensing material at the local pressure of the bath. The rate of condensation is then controlled by the ability of the liquid phase to transport the energy of condensation from the gas-liquid interface to the ambient bath. The temperature differential for this transport process is $T_s - T_x$.

Assuming an axially symmetric flow and employing the coordinate system illustrated in Figure 3, conservation of vapor mass requires

$$d\dot{m}/dx' = -2\pi r'R. \tag{1}$$

The rate of condensation R is given by the interface boundary condition requiring the local rate of energy release through condensation to be equal to the local rate of energy transfer to the ambient bath

$$h_{fg}R = h(T_s - T_x) \tag{2}$$

where h is the local heat transfer coefficient for the liquid phase and h_{fg} is the energy release of condensation. The local vapor mass flow rate is related to the cavity radius and local mass velocity G through the one dimensional mass flux equation

$$\dot{m} = \pi r'^2 G. \tag{3}$$

Substituting Equations (2) and (3) into Equation (1), normalizing and introducing a dimensionless distance variable yields

$$d(\dot{m}/\dot{m}_0)^{1/2}/dx = -(G/G_0)^{1/2} SB \tag{4}$$

where

$$B = C_p(T_s - T_x)/h_{fg} \tag{5}$$

and

$$S = h/C_pG. \tag{6}$$

The parameter B defined in Equation (5) represents a dimensionless driving potential for the condensation process. The transport modulus, S defined in Equation (6) is analogous to the familiar Stanton number of convective heat transfer. It is unorthodox, however, since the present transport modulus employs the vapor mass velocity while the heat transfer coefficient and specific heat pertain to the liquid phase. This choice is convenient since the momentum flux providing the convective flow originates in the vapor phase while the heat transfer resistance lies in the liquid phase. Since conservation of mass implies that the mass velocities of both phases are of the same order of magnitude near the cavity, it would be expected that the values of the present transport modulus would be similar to those of the more conventional definition.

The boundary conditions on Equation (4) are

$$x = 0, \ \dot{m}/\dot{m}_0 = 1; \quad x = X, \ \dot{m}/\dot{m}_0 = 0$$

where X is the dimensionless penetration length of the cavity.

Exact integration of Equation (4) is not possible without detailed information on the variation of G and S along the cavity. However, assuming that appropriate mean values can be chosen for these quantities, Equation (4) can be integrated

STYLE	D (m)	L_i/D	L_o/D	δ
FLAT-HEAD	.00040	34	–	–
	.00079	32	–	–
	.00158	20	–	–
	.00376	20	–	–
	.00635	17	–	–
	.00950	16	–	–
CONICAL	.00158	34	25	8°
	.00367	24	15	7°
	.00635	19	10	6°

Fig. 2. Schematic diagram of injector heads.

TABLE 1. EXPERIMENTAL DATA

T_∞ (K)	B	G_0 (kg/s·m²)	X	$P_c \times 10^4$ (N/m²)
0.00040 m flat head injector				
347.8	0.0473	1141	26.0	68.9
342.8	0.0574	744	18.0	41.4
340.4	0.0613	1141	22.0	68.9
340.0	0.0621	955	22.0	55.2
0.00079 m flat head injector				
301.5	0.1341	660	7.5	48.3
301.7	0.1330	1146	11.0	86.2
301.9	0.1323	1577	12.0	120.0
302.0	0.1320	2044	12.0	157.2
327.6	0.0855	678	10.0	49.6
327.4	0.0851	1100	16.5	82.7
327.5	0.0849	1632	17.0	124.1
327.5	0.0864	2044	17.0	157.2
349.0	0.0456	641	15.0	46.9
0.00158 m flat head injector				
325.3	0.0900	848	10.0	47.2
324.2	0.0925	664	9.0	40.7
324.1	0.0933	515	8.0	33.1
324.1	0.0936	378	5.0	27.6
316.5	0.1064	745	7.0	44.8
316.7	0.1074	584	6.5	33.8
340.1	0.0619	848	11.5	47.6
340.0	0.0623	744	11.5	44.8
340.0	0.0626	664	12.5	40.7
339.8	0.0629	607	10.5	37.9
339.7	0.0636	516	9.5	33.1
339.5	0.0641	378	11.0	27.6
350.0	0.0434	848	14.0	47.2
349.8	0.0439	745	15.5	44.8
349.7	0.0444	664	12.5	40.7
349.3	0.0451	607	18.0	37.9
348.9	0.0462	516	16.5	33.1
348.4	0.0473	378	8.5	27.6
0.00376 m flat head injector				
318.9	0.1024	619	7.5	36.2
318.3	0.1047	527	6.3	32.1
318.6	0.1036	466	6.5	28.6
319.9	0.1008	424	5.8	26.9
341.8	0.0592	624	13.5	38.3
342.3	0.0586	516	11.3	32.8
342.7	0.0579	464	12.0	29.0
342.9	0.0574	424	11.5	26.9
353.2	0.0378	624	16.5	38.3
353.4	0.0375	524	15.8	32.4
352.3	0.0396	470	14.0	29.3
352.3	0.0397	413	15.5	26.5
306.4	0.1250	1255	10.5	77.9
307.9	0.1225	957	9.8	62.1
309.0	0.1213	682	7.8	44.1
309.9	0.1195	447	6.5	31.0
337.7	0.0664	1255	13.8	77.9
338.8	0.0645	957	14.8	62.1
339.5	0.0636	682	13.8	44.1
340.2	0.0623	447	12.3	31.0
352.3	0.0389	1255	28.0	78.6
352.7	0.0385	957	21.2	62.1
353.0	0.0381	682	18.5	44.1
353.2	0.0377	447	15.3	31.0
0.00635 m flat head injector				
318.6	0.1036	458	6.5	31.7
321.7	0.0967	723	9.5	50.3
325.0	0.0904	967	12.8	67.6
330.0	0.0802	1132	13.0	79.3
333.4	0.0755	458	8.5	31.7

TABLE 1. (Cont.)

| T_∞ (K)	B	G_0 (kg/s·m²)	X	$P_c \times 10^4$ (N/m²)
336.6	0.0686	723	13.5	50.3
340.4	0.0615	967	15.5	67.6
344.0	0.0543	1132	25.0	79.3
348.9	0.0461	458	12.3	31.7
351.3	0.0411	723	16.2	50.3
318.4	0.1030	644	8.0	44.8
322.4	0.0953	816	9.8	57.2
326.9	0.0867	888	10.5	62.1
340.8	0.0609	644	12.5	44.8
343.5	0.0557	816	14.5	57.2
346.8	0.0494	888	18.2	62.1
349.6	0.0442	967	18.5	67.6
352.8	0.0378	1132	24.5	79.3
355.5	0.0331	816	25.5	57.2
357.3	0.0297	888	25.0	62.1
328.8	0.0826	1132	12.5	79.3
342.8	0.0565	1132	15.5	79.3
348.3	0.0363	723	19.8	50.3
349.8	0.0443	458	13.0	31.7
314.4	0.1109	530	6.9	36.5
316.3	0.1082	464	6.5	32.4
318.2	0.1043	411	6.1	29.0
320.8	0.0999	379	5.6	26.5
341.2	0.0603	530	11.4	36.5
342.9	0.0577	464	11.5	32.4
337.7	0.0673	404	8.8	27.9
339.4	0.0641	424	9.5	29.6
317.2	0.1045	1160	14.2	85.5
321.5	0.0961	1339	16.7	100.0
326.4	0.0865	1619	24.5	120.7
331.5	0.0773	1848	26.0	139.3
338.0	0.0648	2034	30.0	153.8
343.5	0.0554	1160	23.0	86.2
323.4	0.0917	2034	24.7	153.8
335.7	0.0697	1339	22.7	100.0
340.8	0.0598	1619	26.5	120.0
344.8	0.0507	1862	29.5	140.7
348.1	0.0468	1160	30.2	85.5
351.0	0.0409	1277	33.5	95.1
0.00950 m flat head injector				
328.7	0.0822	1764	20.7	151.7
339.7	0.0621	1578	21.3	134.4
348.8	0.0453	1324	25.6	110.3
352.8	0.0378	1604	30.0	136.5
327.0	0.0856	1337	16.3	111.7
340.2	0.0611	1764	22.6	151.7
0.00158 m conical injector				
302.4	0.1342	527	8.0	31.7
302.5	0.1332	676	4.5	44.5
302.9	0.1321	779	6.0	53.8
303.4	0.1303	894	7.0	57.9
333.0	0.0760	539	7.5	33.1
333.0	0.0760	681	10.0	45.5
333.0	0.0755	779	10.5	53.8
333.0	0.0750	894	12.0	57.9
350.7	0.0428	539	16.0	34.5
350.3	0.0427	894	20.5	57.9
0.00635 m conical injector				
312.8	0.1141	531	7.0	36.5
314.9	0.1108	458	7.0	33.1
316.9	0.1069	408	6.1	29.6
318.7	0.1036	375	5.6	27.2
323.7	0.0943	332	5.3	24.1
336.0	0.0706	524	11.8	35.9
337.2	0.0685	458	10.7	33.1
338.4	0.0659	408	11.5	29.6
339.4	0.0645	381	8.7	27.6
349.8	0.0441	531	19.8	36.5
351.1	0.0420	456	19.3	33.8
352.3	0.0396	408	17.3	29.6
353.2	0.0381	381	14.7	27.6
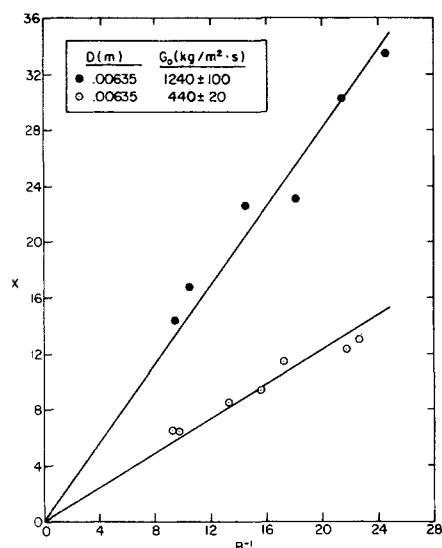
Fig. 4. Variation of dimensionless cavity length with B.

TABLE 1. (Cont.)

0.0112 m convergent-divergent injector

| 345.0 | 0.0502 | 642 | 16.3 | 131.0 |

0.0101 m convergent-divergent injector

| 342.1 | 0.0554 | 588 | 16.1 | 100.0 |

to yield the following approximate expression for penetration length

$$XB = (G_0/G_m)^{1/2}/S_m . \qquad (7)$$

Barring any strong influence of B on the right hand side of Equation (7), this equation suggests that the dimensionless penetration length is inversely proportional to the driving potential for the condensation process. The mass velocity ratio in Equation (7) G_0/G_m relates the injector exit mass velocity to some mean mass velocity representative of the cavity as a whole. While the injector exit mass velocity may be readily determined from the injector geometry and mass flow rate, the mean mass velocity remains to be specified.

For a condition where the injector is just adapted, the vapor mass velocity decreases along the length of the cavity through momentum exchange with the surrounding liquid. When the injector is underexpanded, in addition to frictional effects, the mass velocity decreases through external expansion of the vapor beyond the injector exit. In view of the complexities of these processes, a constant value of G_m was chosen to normalize all the data, rather than attempting to assign a value of G_m appropriate to each test condition. This value was taken to be equal to the critical vapor mass velocity at the ambient bath pressure of the present tests 275 kg/m² · s. Since all the present data was taken with choked injector flows, this value is at least representative of the order of magnitude of the mass velocities in the cavity.

With the value of G_m specified, the remaining effects are transferred to the transport modulus S_m. This factor must be determined empirically from experimental data. In general, this transport modulus should be influenced by a variety of factors which control the turbulence and shape characteristics of the cavity (G_0/G_m, B, Reynolds number, surface tension, Prandtl number, liquid-vapor density ratio, etc.).

RESULTS AND DISCUSSION

For all the tests, the driving potential for condensation was computed at the hydrostatic ambient pressure at the centerline of the injector (within 3% of atmospheric pressure). Only choked injector flows were considered for correlation of the data in order to avoid the complications of unsteady jet operation.

The influence of the condensation driving potential on the cavity length was examined by conducting tests at a relatively fixed injector exit mass velocity for various bath temperatures. Figure 4 illustrates results for a flat head injector at two different mass velocities. The dimensionless cavity length is plotted against the reciprocal of B, which is the dependence suggested by Equation (7) in the absence of any influence of B on the right hand side of the equation. The results indicate that the reciprocal relationship is approximately satisfied.

The data of Figure 4 also points to a substantial influence of injector exit mass velocity on cavity length. The influence of mass velocity is examined further in Figure 5 for flat head and conical injectors. On the figure the dimensionless cavity length is plotted against the injector exit mass velocity normalized by the critical mass velocity at the pressure of the bath. For the tests shown, the value of B was not quite constant but fell in the relatively narrow range 0.1020 ± 0.0100.

The results for flat-head and conical injectors are seen to be nearly the same in Figure 5. Similar agreement between the two injector types was found throughout the test range. It is notable that other phenomena involving gaseous injection into liquids have shown a similar lack of dependence on external injector geometry (9).

A number of general correlations of the data were attempted by the method of least squares. A total of 128 experimental observations, including both flat head and conical injectors were employed in these computations. These results considered injector diameters in the range 0.00040-0.0095m, injector exit mass velocities in the range 332-2050 kg/m² · s, (G_0/G_m in the range 1.2-7.4), Reynolds numbers in the range 2-150 × 10⁴ and bath temperatures from 301-352°K (B in the range 0.028-0.135).

In studying the turbulent condensation of a high velocity vapor on a subcooled liquid jet, Linehan and Grolmes (10) found that the assumption of a constant Stanton number for the process gave a reasonable correlation of their data (although the range of this data was relatively limited). Motivated by the results of Linehan and Grolmes, correlation attempts began by assuming that S_m was a single empirical constant. The resulting correlation was found to be

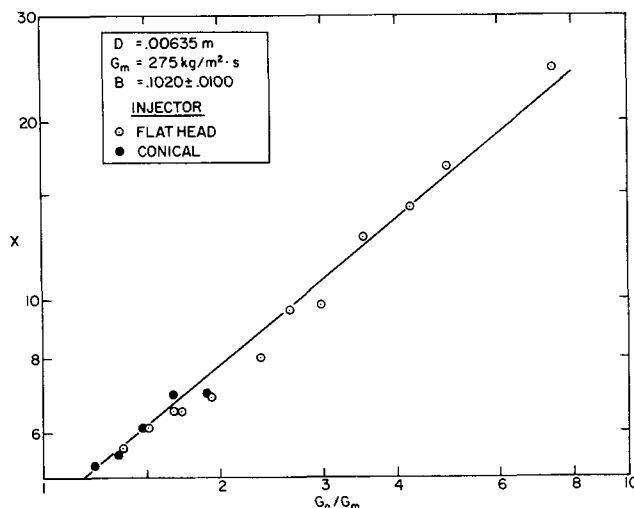$$XB = (G_0/G_m)^{1/2}/1.932 . \qquad (8)$$

Fig. 5. Variation of dimensionless cavity length with mass velocity ratio.
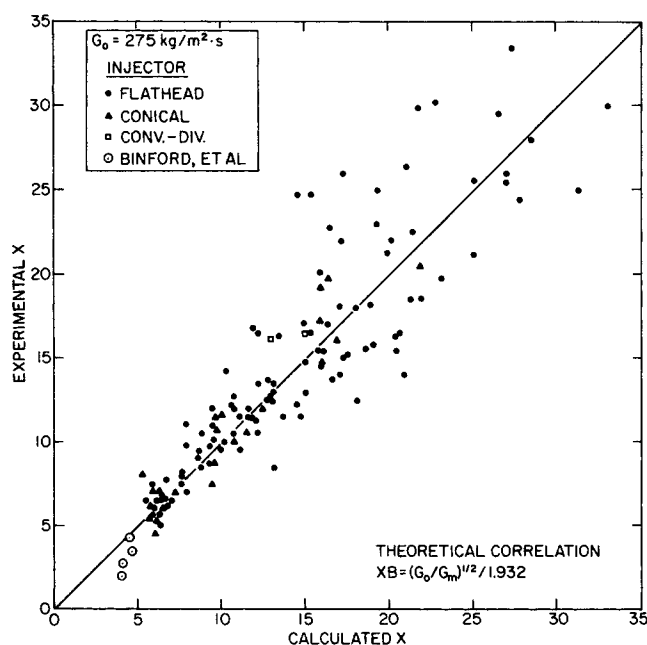
Fig. 6. Comparison of experimental penetration lengths with values calculated from Equation (8).

The average of the absolute deviations of the experimental penetration lengths from the values computed by Equation (8) was 13.6%. Figure 6 illustrates the comparison between the computed and experimental values of X for both flat-head and conical injectors.

Binford et al. (6) also obtained data with constant area injectors and the four choked flow observations from these experiments are compared as well with Equation (8) in Figure 6. These tests employed steel tube injectors, extending into the liquid bath, having inside diameters of 0.0109 and 0.0172 m at a bath temperature of 305°K. This data is also in fair agreement with Equation (8). The largest discrepancies occur when the injector is just choked and the experimental results are more likely to be influenced by oscillatory injector behavior.

Some limited results are also presented in Figure 6 for two convergent-divergent injectors tested during the present investigation. Both of these injectors had throat diameters of 0.00635 m. with 15° conical divergent sections. The design inlet pressures of these injectors, for adapted operation, were 1×10^6 and 1.31×10^6 N/m.^{2} with exit diameters of 0.0101 and 0.0112 m., respectively. Static pressure measurements were made at the exit plane of these injectors to insure adapted operation. While the data is limited, the results indicate that the convergent-divergent injectors can be correlated in the same manner as the constant area injectors.

For values of G_0/G_m near unity, the constant 1.932 can be identified with the Stanton number of the present experiments (if it is accepted that the injector exit mass velocity is representative of cavity mass velocities for nearly adapted injector operation). This yields condensation heat transfer coefficients on the order of 2×10^6 J/m$^2 \cdot$s$\cdot$K at the sonic vapor mass velocity condition. At comparable vapor mass velocities, Linehan and Grolmes (10) found condensation heat transfer coefficients of the same order of magnitude for the turbulent condensation of a high velocity vapor on a subcooled liquid jet. It is notable that the heat transfer coefficients for these condensation processes across free turbulent surfaces are considerably higher than the values usually stated for turbulent condensation near tubes and flat plates. For example, the Carpenter and Colburn correlation (12) for turbulent condensation

in tubes yields heat transfer coefficients almost an order of magnitude lower than the present values at comparable conditions (conservatively assuming a pipe friction factor of 0.1).

A slightly improved correlation of the data can be obtained by removing the restrictions on property powers implied by Equation (7) prior to proceeding with a least squares fit. Assuming that the penetration length is only a function of B and the mass velocity ratio, yields the following expression

$$XB = 0.7166B^{0.1689} \ (G_0/G_m)^{0.6446} \qquad (9)$$

The multiple correlation coefficient for Equation (9) was 0.950 with an average absolute deviation between the measured and predicted values of penetration length of 11.7%. The standard deviations of the powers of B and the mass velocity ratio on the right-hand side of Equation (9) were 0.0342 and 0.0273, respectively.

Replacing the mass velocity ratio with the injector exit Reynolds number resulted in a poorer correlation (multiple correlation coefficient of 0.781). The most complex correlation considered in the calculations included B, mass velocity ratio, injector exit Reynolds number, Prandtl number at the average film temperature and the ratio of liquid viscosities at the cavity surface and in the bulk liquid. The inclusion of all these factors resulted in only a minor increase in the accuracy of the correlation (multiple correlation coefficient of 0.954).

CONCLUSIONS

For steam injection into water at atmospheric pressure, Equation (9) provided an estimation of cavity length with an error of 11.7% over a rather extensive range of experimental variables. The equation is suitable for choked injector flow at values of dimensionless driving potential no less than 0.028. Unchoked flow causes oscillatory injector behavior and very low values of the driving potential gives rise to cavity breakup and buoyancy effects which invalidate the correlation. The correlation appears to be satisfactory for a variety of injector geometries; constant area flat-head, conical and tube injectors as well as convergent-divergent injectors were examined during the investigation.

The use of an approximate theoretical model indicated that the results could be correlated with nearly the same accuracy by assuming that S_m in Equation (7) was a constant. Under conditions where this transport modulus could be associated with the Stanton number; the corresponding heat transfer coefficients of the present investigation were found to be of the same order of magnitude as that encountered in other highly turbulent transport processes across free liquid-vapor interfaces. However, these heat transfer coefficients were found to be about an order of magnitude greater than those encountered in turbulent condensation within tubes, for comparable conditions.

The shape of the cavity was found to be a function of degree of expansion in the injector. For an adapted injector the maximum cavity diameter was only slightly larger than the injector exit diameter. For underexpanded injectors, the maximum cavity diameter was greater than the adapted case, while for overexpanded injectors the cavity diameter would tend to decrease near the injector exit.

NOTATION

B = dimensionless condensation driving potential, $C_p(T_s - T_x)/h_{fg}$

C_p = liquid specific heat, J/kg·K

D = injector diameter, m

G = vapor mass velocity, kg/m²·s

h = heat transfer coefficient, J/m²·s·K

h_{fg} = heat of condensation, J/kg

L = cavity length, m.

$\dot{m}$ = vapor mass flow rate, kg/s

P_c = chamber pressure, N/m²

r' = cavity radius, m

R = rate of condensation, kg/m²·s

S = dimensionless transport modulus, $h/G\,C_p$

T_s = saturation temperature, °K.

T_x = bath temperature, °K.

x' = axial distance, m.

x = dimensionless axial distance, $2x'/D$

X = dimensionless cavity length, $2L/D$

Subscripts

m = mean value for cavity

0 = injector exit conditions

LITERATURE CITED

1. Liebson, I., E. G. Holcomb, A. G. Cacosa, and J. J. Jormic, AIChE J., 2, 296 (1956).
2. Sullivan, S. L., B. W. Hardy, and K. D. Holland, AIChE J., 10, 848 (1964).
3. Davidson, L., and A. E. Amick, AIChE J., 2, 337 (1956).
4. Boehm, J., Gesundh.-Ing., 591-595 (1938).
5. Glikman, B. F., Repts. of Academy of Sciences USSR, Div. of Technical Sciences, Energetics Autom., No. 1, 39-44 (1959).
6. Binford, F. T., L. E. Stanford, and C. C. Webster, Oak Ridge National Laboratory, ORNL-4374, UC-80-Reactor Technol., 234-250 (1968).
7. Kerney, P. J., Ph.D. thesis, Pennsylvania State Univ. (1970).
8. Benedict, R. P., J. Eng. Power, 21 (1969).
9. Abdel-Aal, H. K., G. B. Stiles, and C. D. Holland, AIChE J., 12, 174 (1966).
10. Linehan, J. H. and M. A. Grolmes, 4th Intern. Heat Transfer Conf., Paris, France (1970).
11. Eckert, E. F. G., and R. M. Drake, Jr., "Heat and Mass Transfer," McGraw-Hill, New York (1959).
12. Carpenter, E. F., and A. P. Colburn, Inst. Mech. Eng. ASME, Proc. General Discussion on Heat Transfer, 20 (1951).

Ecological Aspects of Combustion Devices (with Reference to Hydrocarbon Flaring)

J. SWITHENBANK

Department of Chemical Engineering and Fuel Technology
University of Sheffield, Sheffield, England

Some fundamental factors controlling the emission of pollutants by an industrial combustion system are illustrated by reference to gaseous hydrocarbon flare stack combustion. The formation of smoke (soot), radiation, and nitric oxide may be controlled by limiting of the premixed fuel air ratio to moderately rich mixtures. The factors which determine the design of a suitable Coanda mixer are shown to be area ratio, density ratio, and pressure ratio. An important pollutant for large burners is the combustion roar. Fuel type and mixture ratio only affect the combustion noise output by about 5 db. The dominant factor in the generation of this noise is the burner turbulence, which can be controlled to reduce the combustion roar by up to 20 db.

Burner cost considerations lead to the current use of simple flare tips; however, the eventual use of more technically sophisticated low pollution units is inevitable.

Although most fuels will burn readily in air, when we wish to use the combustion process for some technological purpose the manner in which the fuel, air, and combustion products are brought together requires careful control. Thus, even the Pueblo Indians used an air deflector to control the air flow to the fire used to heat their dwellings. The next step taken early in the industrial revolution was the use of a secondary air supply above a burning solid fuel bed to consume combustible gases formed during pyrolysis of the fuel and thus achieve almost 100% combustion efficiency. Unfortunately, the overall process must

be efficient, and the addition of excess air to assist in achieving complete combustion means the loss of heat due to the increased flow of hot gases through the flue. The optimization of the system therefore requires careful design of the combustor to achieve complete combustion with the minimum quantity of excess air.

Our concept of the overall system has now expanded to include the environment as well as the process, and the combustion designer must now reduce the emission of pollutants to an acceptable level. The major pollutants are: 1. particulate, for example, smoke; 2. gaseous, for example,